

# Integrated Soft Optoelectronics for Wearable Health Monitoring

Shantonu Biswas,\* Yitian Shao, Taku Hachisu, Tung Nguyen-Dang, and Yon Visell\*

Recent developments in stretchable electronics hold promise to advance wearable technologies for health monitoring. Emerging techniques allow soft materials to serve as substrates and packaging for electronics, enabling devices to comply with and conform to the body, unlike conventional rigid electronics. However, few stretchable electronic devices achieve the high integration densities that are possible using conventional substrates, such as printed rigid or flexible circuit boards. Here, a new manufacturing method is presented for wearable soft health monitoring devices with high integration densities. It is shown how to fabricate soft electronics on rigid carrier substrates using microfabrication techniques in tandem with strain relief features. Together, these make it possible to integrate a large variety of surface mount components in complex stretchable circuits on thin polymer substrates. The method is largely compatible with existing industrial manufacturing processes. The promise of these methods is demonstrated by realizing skin-interfaced devices for multimodal physiological data capture via multiwavelength optoelectronic sensor arrays comprised of light emitting diodes and phototransistors. The devices provide high signal-to-noise ratio measurements of peripheral hemodynamics, illustrating the promise of soft electronics for wearable health monitoring applications.

One of the most remarkable advances in healthcare and medicine has been the development and application of new electronic methods for monitoring the physiological state of the body. Emerging research in healthcare monitoring, health-related internet-of-things (IoT), body area networks, and wearable computing may amplify benefits that can be achieved in health monitoring by realizing electronic systems that can be worn on the body in unrestricted environments. Wearable electronic devices for healthcare monitoring have been commercially available for several decades.<sup>[1]</sup> Today, they include a growing array of consumer products, including smart watches.<sup>[2]</sup> Similar technologies are used in athletics, clinical health monitoring, and medical diagnosis.<sup>[3]</sup>

Among the most commonly used non-invasive technologies for health monitoring are optoelectronic devices. Such technologies are also widely being used in bioengineering and medicine as tools for diagnosis and physiological data capture. This is possible due to the myriad ways in which light transmission in living tissues

is influenced by physiological and mechanical processes.<sup>[4–6]</sup> In addition, optoelectronic devices are often robust and miniaturizable, making it possible to realize high integration density, multifunctional devices.<sup>[7]</sup>

Health monitoring often benefits from intimate contact between sensors and the body surface. In noninvasive applications, sensors must often be maintained in intimate contact with the skin. However, the compliance of soft body tissues contrasts greatly with the inextensibility of most electronic devices. This can adversely affect body tissues, especially when devices are worn for long durations. It can also limit device functionality, since conforming contact with the skin can degrade over time.<sup>[8]</sup> Thus, there is a need for electronic healthcare monitoring technologies that can stretch to conform compliantly to body surfaces. The most important factor limiting the stretchability of existing devices is the use of rigid materials as bulk carrier substrates or packaging.<sup>[9,10]</sup>

Motivated by these considerations, several research groups have proposed methods for realizing stretchable wearable electronics that conform to the shape of the human body.<sup>[11–14]</sup> Many proposed technologies, including epidermal electronic devices<sup>[15]</sup> and similar inventions,<sup>[16–18]</sup> are thin and highly


Dr. S. Biswas, Dr. T. Nguyen-Dang, Prof. Y. Visell  
California NanoSystems Institute  
University of California  
Santa Barbara, CA 93106, USA  
E-mail: sbiswas@ucsb.edu; yonvisell@ucsb.edu

Y. Shao, Prof. Y. Visell  
Department of Electrical and Computer Engineering  
University of California  
Santa Barbara, CA 93106, USA

Dr. T. Hachisu  
Faculty of Engineering, Information and Systems  
University of Tsukuba  
Tsukuba, Ibaraki 305-8573, Japan

Dr. T. Nguyen-Dang  
Center for Polymers and Organic Solid  
University of California  
Santa Barbara, CA 93106, USA

Prof. Y. Visell  
Media Arts and Technology Program  
University of California  
Santa Barbara, CA 93106, USA

 The ORCID identification number(s) for the author(s) of this article can be found under <https://doi.org/10.1002/admt.202000347>.

DOI: 10.1002/admt.202000347

conformable, but are often compromised in robustness, which can preclude reuse or lead to premature failure. Another recent research thrust in soft electronics is hybrid electronic devices that combine soft, robust carrier packaging with conventional miniature surface mount electronic components.<sup>[10,19]</sup> This can facilitate conformability and robustness, allowing devices to be used for long durations, or in repeated applications. This can decrease costs and reduce environmental impact.<sup>[20,21]</sup>

Among others, one promising application area for such soft and conformable health monitoring devices is in the noninvasive measurement of physiological processes. Recently, several technologies for performing physiological measurements via body-worn conformable devices have been reported in health monitoring and diagnosis.<sup>[15,16,20,22]</sup> Many of these have been restricted to passive sensing or recording functionalities.<sup>[15]</sup> Applications of active electronic components have generally been restricted to simple devices with limited functionality,<sup>[23]</sup> due to the sensitive nature of the fabrication methods that are used to produce them, which preclude manufacturing at scale.<sup>[21]</sup> Few manufacturing methods for soft electronic devices have been proposed that can achieve integration densities that approach those that can be achieved with even low-cost printed circuit board (PCB) processes.<sup>[19,24]</sup> Some of the requirements that make it challenging to design such processes include compatibility with high temperature processing, amenability to accurate alignment and registration, and compatibility with precise assembly of multiple surface mount components (SMDs) over large areas.

In this communication, we report methods for manufacturing robust, wearable stretchable electronic devices, with applications in healthcare monitoring. To achieve this, we present new methods for the fabrication of stretchable electronics that adapted from conventional planar fabrication techniques. Such techniques make extensive use of rigid carrier substrates, which can enable facile fabrication of circuits with greater densities than are practical using previous methods. Using our approach, it is possible to fabricate stretchable circuits with surface areas that can be scaled to meet application requirements using commercially available active or passive surface mount (SMD) components. A critical element of our approach is that all fabrication is performed while the circuits are supported on rigid substrates. Only the final step is the circuit transferred to a soft polymer substrate. This makes it possible to use high temperature processing, to perform accurate registration, and to achieve large surface areas with high integration densities, exceeding what can be achieved with prior methods for soft electronics fabrication, and approaching those that are possible with conventional PCBs. The devices produced by our process involve encapsulation in a transparent, soft polymer membrane that is flexible, stretchable, and can conform to the body. Our method is compatible with a large variety of soft polymers.

We demonstrate the promise of this approach by fabricating wearable optoelectronic devices for healthcare monitoring based on arrays of multiwavelength (visible and infrared) light emitting diodes and (visible and infrared) phototransistors. As we demonstrate, these devices may be worn on the skin and operated in transmission or reflection mode in order to capture multimodal physiological signals reflecting the state of subcutaneous tissues, including peripheral hemodynamics related to blood circulation or cardiac function.

Our research makes it possible to design and fabricate highly functional soft, stretchable electronic devices for health monitoring. We introduce a method of manufacture that can achieve high integration densities and can integrate commercially available active SMD electronic components. In our process the circuit is supported on a rigid carrier substrate (silicon wafer) until the very final stage, in which it is transferred to a soft polymer substrate. This allows our process to accommodate important manufacturing requirements, including high-temperature processing, and optical registration for precise component placement.

We have used this method to design and fabricate functional health monitoring devices based on multimodal optical sensor arrays (**Figure 1**). These devices integrate arrays of multiwavelength (visible and infrared) light emitting diodes, phototransistors, and other SMD components. By injecting light from multiple sources and sensing reflected or transmitted light at multiple wavelengths, a variety of signals may be noninvasively captured reflecting physiological processes and tissue states, including peripheral hemodynamics, heart rate, or tissue strain. Stretchability allows these devices to be integrated in compliant form factors, such as wrist bands or rings, that may be worn on the body (**Figure 1A**). Mechanical stretchability also facilitates consistent proximate contact with body surfaces or tissues and thus stable measurement conditions.

We engineer these optoelectronic devices using transparent, stretchable polymer substrates (e.g., Clear Flex, Smooth On, Inc.), which we selected for excellent light transmission. However, in other devices, any moldable polymer resin may be used. The electronics can comprise a number of active or passive components and circuit traces with strain management features (**Figure 1B,C**). These are consolidated within a single active layer encapsulated between two layers of the polymer substrate. In our optical sensing devices, a (1 mm) base polymer layer acts as the substrate for the device, while a thinner polymer layer ( $\approx 100\ \mu\text{m}$ ) provides protective encapsulation at the opposite side. Our process can accommodate other thicknesses, depending on application requirements, due to the support that is provided by the rigid substrate during fabrication (details below and in the Experimental Section). The circuit in the active device layer comprises three different sublayers in a heterogeneous materials stack (**Figure 1B** and inset), including conductive interconnects (circuit traces; Au, thickness:  $10\ \mu\text{m}$ ), solder junctions that bond the SMD components to the pads, and commercially sourced active SMD components. In this arrangement of different sublayers embedded within the 1 mm thick substrate the integration of a very thin layer of transparent polymer at the functional side of the optical SMDs allows light to efficiently pass through (see **Figure S1** in the Supporting Information), which minimizing optical effects of the substrate on the measurements.

We highlight three different arrangements of the optical emitters and detectors in these functional prototypes. The first consists of three infrared (IR) wavelength emitters ( $\lambda_{\text{peak}} = 880\ \text{nm}$ ), one IR phototransistor ( $\lambda_{\text{peak}} = 830\text{--}950\ \text{nm}$ ), three red-green-blue (RGB) wavelength emitters ( $\lambda_{\text{R}} = 619\text{--}624\ \text{nm}$ ,  $\lambda_{\text{G}} = 520\text{--}540\ \text{nm}$ ,  $\lambda_{\text{B}} = 460\text{--}470\ \text{nm}$ ), one visible-wavelength phototransistor ( $\lambda_{\text{peak}} = 450\text{--}610\ \text{nm}$ ); see **Figure 1C** and **Figure S2** (Supporting Information). In many

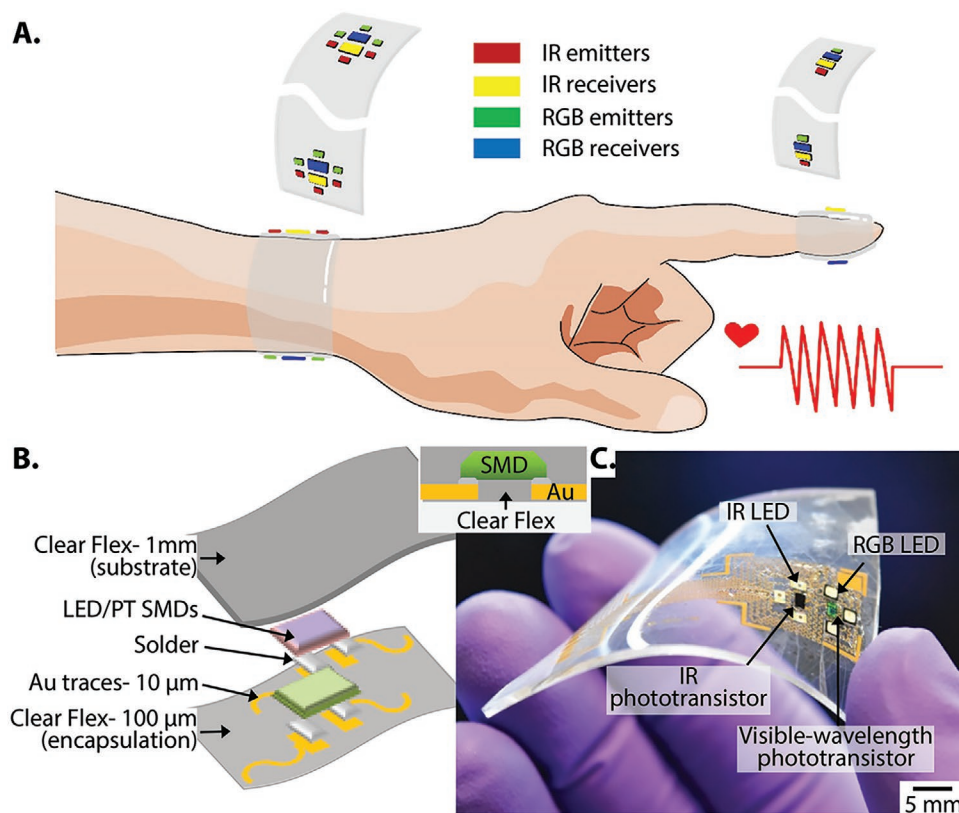


**Figure 1.** A) Schematic illustration of the multimodal optoelectronic sensor arrays mounted at the different locations of the body to record physiological data. B) Schematic device design and C) photograph of such optoelectronic sensor arrays integrated in a transparent and stretchable substrate. IR: infrared, RGB: red-green-blue, LED: light emitting diode, PT: phototransistor, SMD: surface mount device, Au: gold.

devices described in the literature, or integrated in commercial products, red and IR light emitters are often used, because of their distinct absorption coefficients and the variation of absorption with oxygen saturation in the blood.<sup>[5,7,11,22,25]</sup> We also demonstrate a second design that integrates one RGB and one IR emitter, and a third design that integrates one visible-wavelength and one IR phototransistor (see Figure S3 in the Supporting Information). These different exemplary devices show how different arrangements of emitters and detectors may be selected depending on the mounting surface area of the device, the measurement task, and the application configuration and requirements. Multiple emitters operating at different wavelengths, and positioned at different locations, make it possible to capture multiple signals that probe tissues at different wavelengths, or along different optical propagation paths, via a compact device. Applications for such device configurations include photoplethysmographic sensing for physiological measurement or tissue force or strain measurement, among other possibilities.<sup>[26]</sup>

Our first test device includes an arrangement of central phototransistors operating surrounded by an arrangement of LEDs with matching wavelengths (Figure 1C). This isotropic arrangement of emitters and the detectors amplifies the sensitivity of the device by assuring that the phototransistors receive ample light across the measurement range. This effect is enhanced due to the high integration density achieved by our process.

Central to our fabrication method is our adaptation of conventional microfabrication techniques for the fabrication and

assembly of a soft circuit by means of a planar, rigid substrate. This method is significantly different from other methods that use flexible or soft substrates to fabricate and assemble the circuit, because it ensures that the structure is geometrically and mechanically stable during fabrication.<sup>[7,11,15,21,23,27]</sup> This stability makes this method compatible with automated processes such as robotic assembly of surface mount components. The rigid substrates in our exemplary embodiments consist of silicon wafers (diameter: 100 mm). The wafers are coated with a first layer (1  $\mu\text{m}$ ) of polymethyl methacrylate (PMMA) and are subsequently coated with a thicker layer (10  $\mu\text{m}$ ) of polyimide (PI); see Figure 2A and Figure S4 in the Supporting Information. These two materials function as release and sacrificial layers, respectively, which are important steps during fabrication. The adhesion between PMMA (pink layer in Figure 2A) and PI (green layer in Figure 2A) are controlled through physical processes in order to ensure that they are sufficiently mechanically and thermally robust to accommodate the subsequent stages of fabrication, while still being readily separated where required. The PMMA and PI coated Si substrate is subsequently cured in a convection oven (300  $^{\circ}\text{C}$ ,  $\text{N}_2$  atmosphere) for three hours. This endows the substrate with the rigid carrier properties that enable the subsequent processing steps.

This cured substrate is coated with an Au seed layer (thickness: 400 nm) via electron beam evaporation. Photolithography is then applied to pattern this seed layer according to the circuit layout, which is produced via computer aided design, in

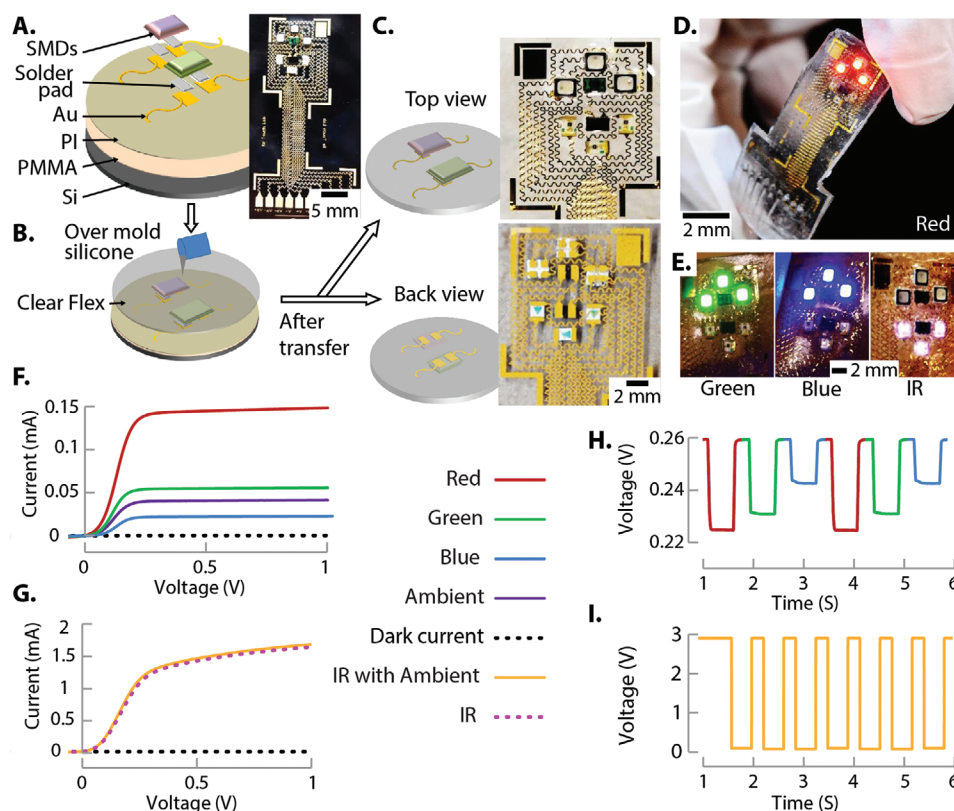


**Figure 2.** Design and functionality of our multimodal optoelectronic sensing devices. A) Functional layers in the device during fabrication of multimodal optoelectronic sensor arrays (Au: gold, PI: polyimide, PMMA: polymethyl methacrylate, PI: polyimide, Si: silicon). The process is based on a planar rigid carrier, and uses adaptations of conventional microfabrication (see inset). B) A transparent soft polymer formed via binary mixture functions as the embedding substrate of the circuit. C) Top and bottom views of the device illustrate the detail achievable using our method. D,E) The LEDs may be selectively illuminated at different IR or visible wavelengths (red, green, blue) during operation following transfer from the rigid carrier. Light is efficiently transmitted through the thin, transparent polymer. Output (I–V) characteristics of F) the RGB and G) the IR LED driven phototransistors. H) The RGB and I) the IR phototransistors respond rapidly and consistently over time.

preparation for electroplating. A 10  $\mu\text{m}$  thick Au layer is produced via electrodeposition using the thin, evaporated Au layer to seed electrodeposition. The residual Au seed layer is chemically removed after electrodeposition, yielding meander-shaped metal interconnects<sup>[28]</sup> on the carrier substrate that are needed to ensure stretchability (see Figure S5 in the Supporting Information). At this stage the substrate is ready for the mounting of active surface mount components (see Figure S6 in the Supporting Information). To assemble the surface mount components, we apply a low melting point alloy solder (melting point: 47  $^{\circ}\text{C}$ ) coating on the assembly pads. This is achieved through lithography and dip coating of the substrate in a molten solder bath. This process allows the alloy to produce a solder coating that is confined to the pad surfaces.<sup>[29]</sup> The SMDs are then placed on the pads. Application of thermal reflow allows the pads, solder, and SMDs to self-assemble due to the reduction in surface energy that is achieved between the molten solder and SMD pads (Figure 2A, inset).<sup>[30]</sup> The device is then tested for functionality. Subsequent stages involve the processing of the stretchable polymer substrate, and do not require any further high-temperature or alignment processing (see Figure S7 in the Supporting Information).

A wide range of polymer elastomers can be used as stretchable substrates. Such materials can be selected to be moldable,

mechanically flexible, soft and stretchable, optically transparent, electrically insulating, sustainable in open environment, and nontoxic, according to application requirements. For the optoelectronic devices presented here, we selected a commercially available transparent, stretchable urethane rubber compound (Clear Flex 50, Smooth-On Inc.) because of its high transparency (refractive index  $\approx 1.48$ ), high stretchability (500%), UV resistance, relatively high tensile strength ( $>1.7$  MPa), and room temperature curability. This polymer is produced via mixing of two resin components in a 1A:2B mass ratio. The circuit supported on the rigid carrier is first treated under ozone for 10 min in order to prime it for bonding. The transparent polymer is then over molded on the circuit according to the thickness that is required based on application needs (Figure 2B). This allows the liquid polymer to automatically fill and align any microscopic gaps in the circuit, and go surround the SMD components, augmenting the adhesion among circuits, SMDs, and stretchable substrate.<sup>[24]</sup> This transparent polymer layer is cured at 60  $^{\circ}\text{C}$  for 1 h. The stretchable device is then removed from the rigid carrier.

Detachment is achieved without any solvent addition due to low interfacial adhesion force between PMMA and PI layers interface.<sup>[24]</sup> The device (circuit and transparent polymer) is readily peeled from the rigid substrate at this interface. The



base PMMA layer is left behind with the Si substrate, while the sacrificial PI layer remains with the transparent polymer. In the final stage, the sacrificial PI layer is entirely removed from the device using  $\text{CF}_4$  and  $\text{O}_2$  plasma processing in an etching chamber. At this stage, the base, conductive surfaces of the circuit are exposed. An additional 100  $\mu\text{m}$  thick transparent polymer layer is spin coated in order to encapsulate and insulate the circuit (Figure 2C). We also determined that this final (bottom) polymer layer increase the mechanical stability of the device, ensuring greater longevity and robustness. The (top) polymer surface is transparent (refractive index 1.495). In addition, the top surface is very thin at the highest points of the emitter and detector SMD components. This ensures that the emitted and detected optical signals are minimally affected by the transparent substrate. Optical emitters (RGB or IR LEDs) are fully functional at this stage, and remain so even the device is bent, stretched, or worn on the skin; our measurements show the performance of the device to be stable with respect to such operations (Figure 2D,E).

We assessed the intrinsic optoelectronic performance of the devices using a controlled optical environment. In one assessment, we coupled two identical optoelectronic devices in a proximal, face-to-face, configuration. We controlled light emission from the LEDs using a microcontroller. We measured output current from the phototransistors via a laboratory parameter analyzer (model 4200A, Keithley Inc.). We computed the device characteristics ( $I$ - $V$  curves) separately for the visible-wavelength phototransistors (Figure 2F) and the IR phototransistors (Figure 2G) by controlling output from the RGB and the IR LEDs respectively. We also characterized the phototransistors by measuring the dark currents they produced (black dotted lines in Figure 2F,G, see Figure S8 in the Supporting Information). Since, no optical filter was applied to the phototransistors, the output current for different light colors varies with measurement conditions. The recorded current for any light color remained consistent over time (Figure 2H,I). The output voltage of the phototransistors was measured against a reference over time for each color LED channel. The curves present consecutively recorded signals from the visible-wavelength (Figure 2H) phototransistor. We achieved this by driving the RGB LED channels for each LED separately via pulse width signal (pulse width: 500 ms, interpulse time: 250 ms) for six cycles each (Figure 2H). We used a similar approach to evaluate the IR phototransistor (Figure 2I). The output voltage measured from all visible and IR LEDs was stable over time, yielding low noise measurements with high signal-to-noise ratio.

Optical sensors are used in diverse applications including medical and health monitoring devices, often exploiting the fact that the propagation of light through biological tissues is modulated by physiological processes to capture health related data.<sup>[22,31]</sup> Optoelectronic devices are valuable for noninvasive physiological measurement since the solid state lighting components can be focused, depending on application requirements, in order to provide microscopic scale resolution. This makes it to probe tissues, organs, or cells.<sup>[25,5-7]</sup> The penetration depth of light in tissue is significant but wavelength-dependent, and thus can be controlled through device design. This is challenging to achieve using other methods, such as electromechanical devices.<sup>[31]</sup>

A wide range of optical bandwidths in the visible or IR ranges can be used depending on application requirements. Here, we show how our devices can perform photoplethysmographic (PPG) sensing of peripheral hemodynamic signals reflecting pulse or other circulatory parameters.<sup>[5]</sup> The PPG method has other applications, including tissue strain or force measurement.<sup>[26]</sup> PPG hemodynamic measurement leverages the tissue-dependent absorption of light, which varies according to local blood volume and oxygenation.<sup>[7]</sup> Absorption varies with the wavelength of the light source.<sup>[27]</sup> This can facilitate multiple measurements via different optical paths and bandwidths.

We first evaluated the optoelectronic PPG sensor during operation in transmission model. In this configuration, light emitted from the LEDs was transmitted through the tissue and captured via phototransistors at the opposing side. To demonstrate how such a device can be made portable, we captured data in real-time via a microcontroller (Figure 3A) with a sampling rate of 1000 Hz (see the Experimental Section). The device employed a pair of LEDs and a pair of phototransistors, each embedded in polymer substrates. The two parts of the device were connected via a soft polymer (EcoFlex 00-30, platinum catalyzed silicone polymer, Smooth-on, Inc.) forming a finger-wearable soft structure (Figure 3B) that readily conformed to the skin. Several properties of the fingernail, including mechanical rigidity, paucity of living cells or nerve endings near the surface, and minimal interfacial water loss, make it attractive for this kind of measurements.<sup>[7]</sup> For these reasons, many commercial devices used in clinical practice employ these easily accessible locations. Except where noted, all measurements were performed in an indoor environment in the presence of ambient light.

The measurements clearly captured the pulse signal via the optical device, and provided low noise measurements for one minute or (Figure 3C, 25 s displayed). The anacrotic phase (systolic) and the catacrotic phase (diastolic) can be readily observed in the data. The pulse also shows the characteristic diastolic notch associated with the closure of the aortic valve.<sup>[32]</sup> Heart rate is also easily obtained from the data, here showing an average rate of  $\approx 70$  beats per minute (BPM; Figure 3D).

This optoelectronic device can also operate in multiwavelength mode, using multiple light sources and detectors. We multiplexed the emitters and detectors for different channels in order to capture multiwavelength measurements that were, at the time-scale of the physiological process, effectively simultaneous. The pulse signal is readily observed in the measurements from each visible or IR channel (Figure 3E). The amplitude of the peripheral pressure, which reflects the systolic peak and diastolic foot of the pulse signal, can be discerned in the signal from each optical measurement band. The IR channel yielded higher amplitudes, due to the reduced optical absorption by tissue at IR wavelengths (Figure 3F).

The integrated soft optoelectronic sensor arrays designed here also can be used to record physiological data in reflection mode, where the device transmits optical signals and records the reflected signals from the biological tissue. To demonstrate this, we use an integrated device with three RGB LEDs, one visible-wavelength phototransistor, three IR LEDs and one IR phototransistor (see Figure 1), which is mounted on the nail of the fingertip (Figure 4A) and a similar set of data is collected in

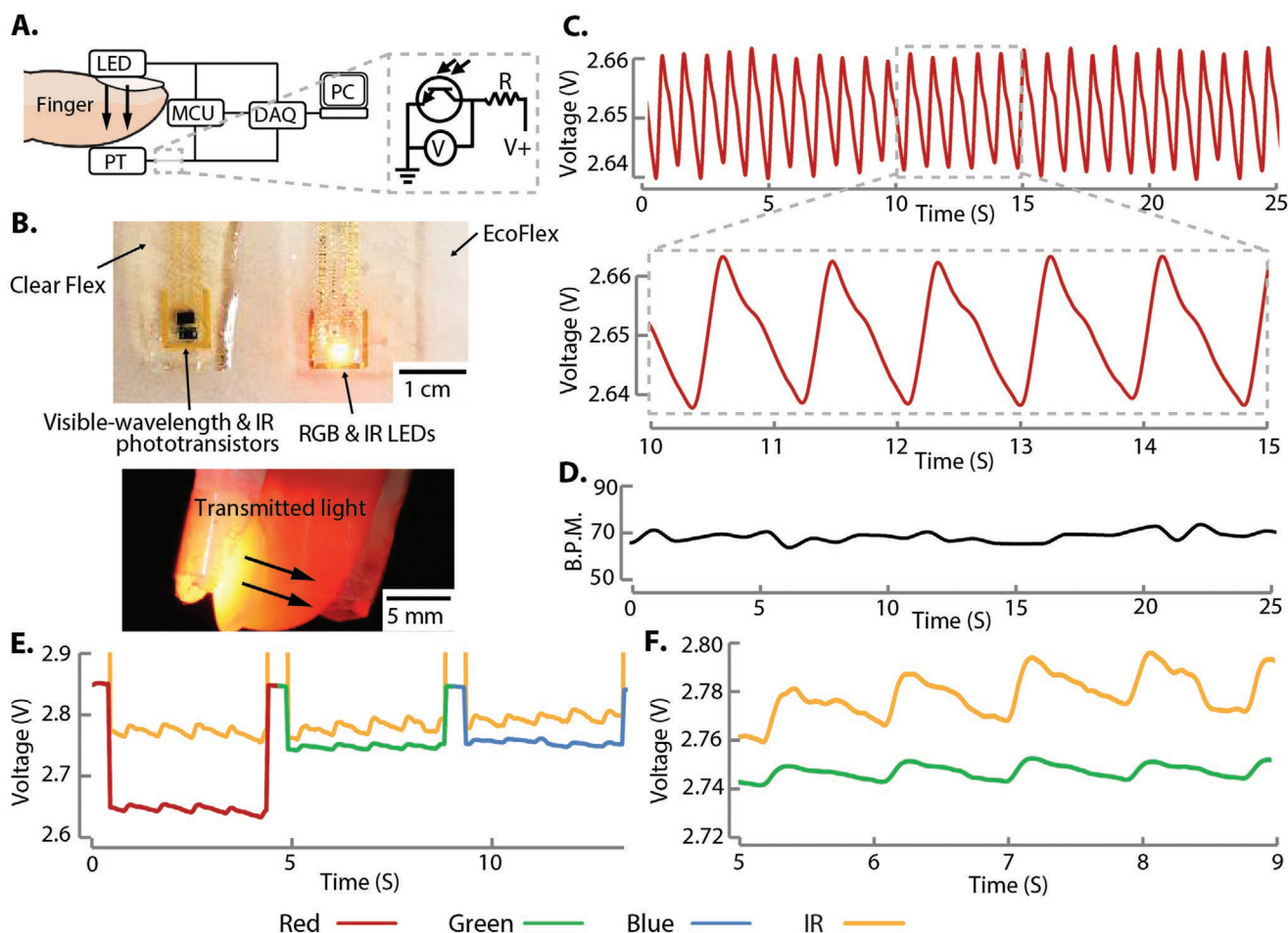


**Figure 3.** Photoplethysmographic (PPG) sensing via a stretchable optoelectronic device operating in transmission mode. A) The device comprises an optoelectronic sensor array worn on two sides of the distal fingertip. Phototransistor voltages reflect the quantity of transmitted light (inset). B) The device comprises two active regions, one worn on each side of the fingertip. C) The output of the phototransistor in response to visible red light emission clearly captures the pulse, from which D) the heart rate (beats per minute) is readily determined. E, F) Green, blue, and IR channels also reflect the pulse signal. LED: light emitting diode, PT: phototransistor, MCU: microcontroller unit, DAQ: data acquisition board, PC: computer.

transmission mode. The recorded signals from the phototransistor present nearly a consistent heart pulse over a time period (Figure 4B). The data from the reflection mode is comparable with the data from the transmission mode. The magnified view of the pulse over five seconds (inset Figure 4B) also shows a similar trend as of the transmission mode and the different phases of the pulse can be recognized as well. The extracted heart pulse rate from this data shows a heart rate of about 70 BPM (Figure 4C) which is nearly same as recorded in the transmission mode while the subject is in steady state. However, the changes in the magnitude of the recorded signals should be noted. In case of the reflection mode, the amplitude (the systolic peak and the diastolic foot) of the recorded signals is reduced by nearly 50% compare to the transmission mode. This is probably because phototransistors in the current device receive more lights in the transmission mode than the reflection mode while being worn in the fingertip.

The heart pulse can be also recorded in reflection mode using different optical signals with different wavelengths. We recorded reflected signals from the tissue using visible-wavelength phototransistors and the IR phototransistors for

different colors (Figure 4D). The extracted results show a comparable heart pulse for red, green, blue, and IR lights. However, one significant difference between the transmission mode and the reflection mode can be noticed from the IR signals (yellow curve in Figures 3 and 4) which is that the reflected IR signals have relatively a low output signal compare to the transmission mode. For example, in transmission mode the recorded voltage for the IR signal ( $\approx 2.75$  V) was higher than the RGB signals (see Figure 3E). Where in the reflection mode, the IR signal ( $\approx 2$  V) is less than the RGB signals (see Figure 4D). This is probably because of the different scattering and absorption coefficient of the living tissues in different wavelengths.<sup>[31]</sup> In the transmission mode, the optical signal is absorbed by the different tissues while passing through the whole finger. On the other hand, the reflection mode detects the signal that is scattered and reflected from tissues.<sup>[31]</sup> Figure 4E shows the magnified view of the recorded signals from blue (top) and IR (bottom) lights in reflection mode.

We further realized embodiments in which the optoelectronic devices are employed in reflection mode. This allows them to be applied at locations of the body in which the emitting and

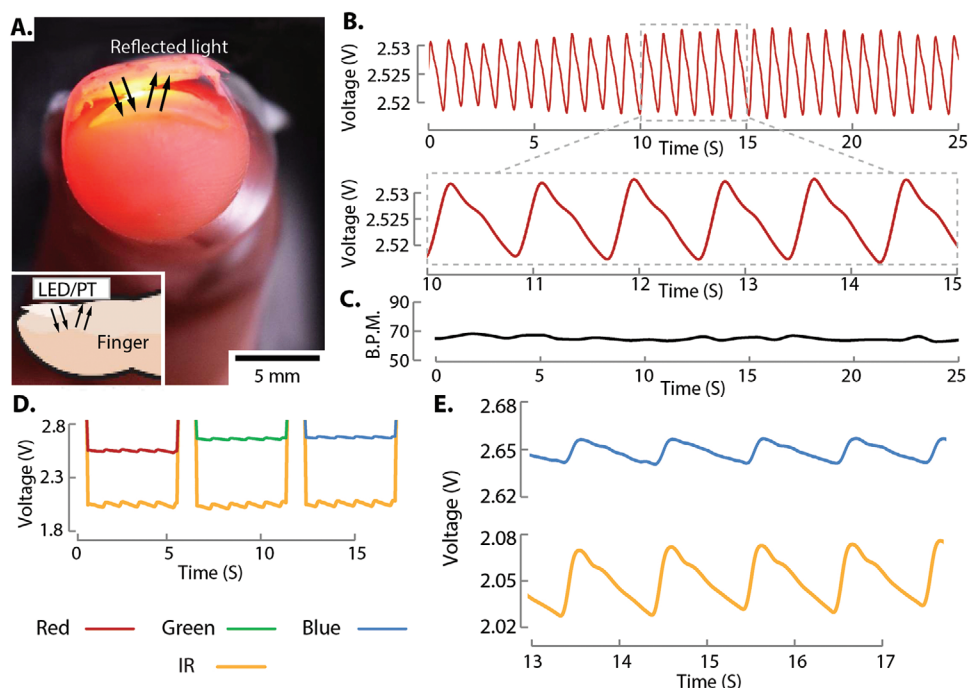


**Figure 4.** A) A photograph and schematic (inset) test set up of the optoelectronic sensor arrays mounted in the fingertip in reflection mode. B) Recorded heart pulses from the multimodal optoelectronic sensor arrays in the reflection mode using red LED while mounted on the fingertip and C) calculated heart beat (BPM) from the recorded pulse. D) Recorded signals from the phototransistors using different lights, and E) magnified view of the recorded signals using IR and blue lights.

detecting components would otherwise bridge a distance too large to provide measurements in transmission mode, facilitating wearable sensing at multiple body locations. We realized these devices using a highly stretchable substrate of silicone

polymer (EcoFlex, Smooth On, Inc.) (**Figure 5A**), yielding devices that can be applied to the skin in a variety of ways, such as via a band worn on the finger, wrist, or upper arm (**Figure 5B**). Pulse signal measurements from this reflection-mode

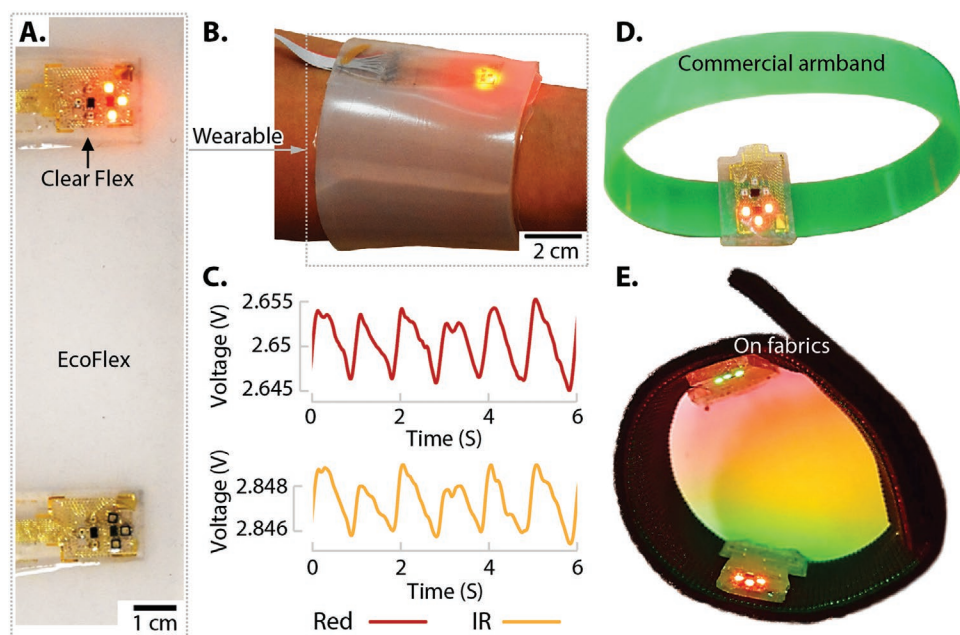


**Figure 5.** A) Photograph of the multimodal optoelectronic device encapsulated within a highly stretchable silicone substrate. B) The device can be worn as a wrist band and C) can be used as a PPG sensor in reflection mode. D,E) Photographs of the optoelectronic sensor arrays embodied in different substrates.



device can be captured via red or IR channel sensors, although the signal amplitudes are lower due to the smaller proportion of light that is reflected back to the phototransistors in the device (Figure 5C).

The design and manufacturing methods presented here can be used to fabricate devices based on a wide variety of polymer substrates that can be mold cast, including (with slight modifications) fabric-backed polymers (Figure 5D). The many possible configurations of these stretchable optoelectronic devices enable such devices to be integrated into a variety of wearable devices or garments for continuous health monitoring (Figure 5E).

Emerging methods for the design of soft, stretchable, and conformable electronic devices hold promise for the creation of new sensing devices for health monitoring, diagnosis, and other applications. These methods can also improve the resilience, safety, and reusability of existing devices. A critical factor that will affect the adoption of these techniques is the scalability of the methods used to fabricate them, including their suitability for realizing complex, integrated devices, higher integration densities, and their compatibility with industrial processes of manufacturing.

Here, we presented a new design and manufacturing method for wearable soft health monitoring devices. Our method can be used to realize stretchable devices for wearable sensing, including health monitoring, with high integration densities. Our process uses a rigid carrier substrate, accessible micro-fabrication techniques, and provides strain relief features, in order to realize stretchable circuits on thin polymer substrates. Together, these make it possible to realize stretchable and wearable circuits that are robust, achieve high integration densities approaching those that are possible with conventional PCBs, can utilize commercially available SMD components, and are compatible with many industrial manufacturing processes. The high stretchability of the resulting devices endows them with great resilience and allows them to sustain conforming contact with curved or soft surfaces, including body tissues.

We demonstrated the potential of this method by realizing multimodal optoelectronic sensor arrays for wearable health monitoring. These devices use tiny visible and IR LEDs and phototransistors embedded within transparent and stretchable polymer substrates. This endows devices stretchability sufficient for them to conform to body surfaces in wearable applications. As we demonstrated, these devices are capable of capturing physiological signals reflecting peripheral hemodynamics and cardiac function with high signal to noise ratio. While we focused on these embodiments and functionalities, the same methods can be used to realize devices integrating acoustic sensors, force sensors, inertial sensors, bioelectronic sensors, among many other possibilities. They hold promise for many applications in invasive or noninvasive health monitoring, medical diagnosis, imaging, haptics, and robotics.

A critical factor that will affect the impact and adoption of emerging stretchable electronic methods are the compatibility of the methods that are used with industry process, the scalability of the methods, and the resilience of the resulting devices. Indeed, clinical applications and industry both demand that such devices meet requirements that go beyond those of lab prototypes. To achieve this, further research is required on materials, manufacturing methods, and design methods. These findings provide an important advance toward the vision of

ubiquitous stretchable electronics for health monitoring. The many uses that this work can enable could improve outcomes and quality of life for millions of people.

## Experimental Section

**Fabrication of Stretchable Optoelectronic Devices:** A thick Si wafer (diameter: 100 mm, thickness: 500  $\mu\text{m}$ , University Wafer) was spin coated with a layer of PMMA (layer thickness: 1  $\mu\text{m}$ , 950 PMMA C9, MicroChem) and with a further layer of PI (layer thickness: 8  $\mu\text{m}$ , PI 2610, HD Microsystem). It was cured in a convection oven at 300  $^{\circ}\text{C}$  for 3 h under  $\text{N}_2$  flow (Blue M Electric). Layers of Ti and Au (thickness: 20 and 400 nm) were deposited on the cured PI layer using electron-beam evaporation (SEC-600-RAP, Cha Industries). The wafer was then patterned for electroplating by photolithography (Mask Aligner MA/BA-6, Karl Suss America) using a positive resist (SPR 220-7.0, Shipley). A layer of Au (thickness: 10  $\mu\text{m}$ ) was then electroplated on the wafer (SEMCON 1000, Technic, Inc.). Unwanted Au and Ti were chemically removed using Au etchant (Gold Etchant TFA, Transene Company, Inc.) and Ti etchant (Titanium Etchant TFTN, Transene Company, Inc.). The wafer was then patterned for soldering by photolithography via positive resist (AZ P4110, Integrated Micro Materials) and baked at 120  $^{\circ}\text{C}$  for 10 min. The pads were dip coated in a solder bath (Belmont #2451, MP 47  $^{\circ}\text{C}$ ) and the resist was removed.

**Assembly of the SMD Components:** The SMD components were assembled on the fabricated substrate using a standard pick-and-place technique. The wafer was heated from the beneath to melt the solder. The surface mount components (IR emitters, APT2012SF4C-PRV Kingbright; IR phototransistor TEMT7100  $\times$  01 Vishay Semiconductors; RGB emitters, CLMVC-FKC, Cree; visible-wavelength phototransistor, TEMT6200FX01, Vishay Semiconductors) were assembled. A subsequent reflow process allowed the components to self-align. The substrate was treated with ozone for 10 min to increase surface adhesion prior to the next step.

**Encapsulation and Device Assembly:** Resin for the transparent silicone polymer (Clear Flex 50, Smooth-On, Inc.) was prepared by mixing part A and part B (mass ratio 1:2). The liquid silicone resin was poured on top of the substrate bearing the assembled components and left to cure overnight at room temperature, followed by 1 h of curing at 60  $^{\circ}\text{C}$ . The cured transparent polymer layer was removed via peeling at the sacrificial PI layer. In a final step, the sacrificial PI layer was removed via dry etching in ICP (40 SCCM  $\text{O}_2$  + 10 SCCM  $\text{CF}_4$ , 150 W RF power, 0.025 mbar; Panasonic E6261, Panasonic Factory Solutions, Japan) for 17 min. At this stage electrical contacts to the device were made via manual soldering. Finally, the device was coated with another layer of transparent polymer to encase the device.

**Wearable Optoelectronic Device Testing:** For functional testing of the optoelectronic device during application to the body, data were captured via an external microcontroller unit (MBED LPC1768) and data acquisition board (DAQ, NI 9205) connected to a computer via a chassis (NI cDAQ-9174) via universal serial bus (USB). The microcontroller synchronously operated each of the LEDs while the DAQ acquired the output signals from the respective phototransistor. All measurements were using a sample rate of 1000 Hz. See Figure 3A. The experiments involving human subjects have been performed with their full, informed consent in accordance with all local laws.

## Supporting Information

Supporting Information is available from the Wiley Online Library or from the author.

## Acknowledgements

The research received financial support through grants from National Science Foundation (NSF-1628831, NSF-1623459, and NSF-1751348).



The authors thank David Bothman (California NanoSystems Institute Microfluidics Lab) for valuable assistance.

## Conflict of Interest

The authors declare no conflict of interest.

## Keywords

health monitoring, optoelectronics, stretchable electronics, wearable electronics, wearable sensors

Received: April 13, 2020

Revised: May 18, 2020

Published online:

- [1] M. Haghi, K. Thurow, R. Stoll, *Healthcare Inf. Res.* **2017**, 23, 4.
- [2] S. Seneviratne, Y. Hu, T. Nguyen, G. Lan, S. Khalifa, K. Thilakarathna, M. Hassan, A. Seneviratne, *IEEE Commun. Surveys Tutorials* **2017**, 19, 2573.
- [3] K. Kaewkannate, S. Kim, *BMC Public Health* **2016**, 16, 433.
- [4] T. Yokota, P. Zalar, M. Kaltenbrunner, H. Jinno, N. Matsuhisa, H. Kitanosako, Y. Tachibana, W. Yukita, M. Koizumi, T. Someya, *Sci. Adv.* **2016**, 2, e1501856.
- [5] C. M. Lochner, Y. Khan, A. Pierre, A. C. Arias, *Nat. Commun.* **2014**, 5, 5745.
- [6] H. Xu, J. Liu, J. Zhang, G. Zhou, N. Luo, N. Zhao, *Adv. Mater.* **2017**, 29, 1700975.
- [7] J. Kim, P. Gutruf, A. M. Chiarelli, S. Y. Heo, K. Cho, Z. Xie, A. Banks, S. Han, K.-I. Jang, J. W. Lee, K.-T. Lee, X. Feng, Y. Huang, M. Fabiani, G. Gratton, U. Paik, J. A. Rogers, *Adv. Funct. Mater.* **2017**, 27, 1604373.
- [8] Y. Wang, T. Hong, L. Wang, G. Li, N. Bai, C. Li, P. Lu, M. Cai, Z. Wu, N. Lu, B. Yu, J. Zhang, C. F. Guo, *Mater. Today Phys.* **2020**, 12, 100191.
- [9] Z. Bao, X. Chen, *Adv. Mater.* **2016**, 28, 4177.
- [10] S. Biswas, J. Reiprich, T. Cohrs, D. T. Arboleda, A. Schoeberl, M. Mozafari, L. Schlag, T. Stauden, J. Pezoldt, H. O. Jacobs, *Adv. Mater. Technol.* **2017**, 2, 1700131.
- [11] J. Kim, G. A. Salvatore, H. Araki, A. M. Chiarelli, Z. Xie, A. Banks, X. Sheng, Y. Liu, J. W. Lee, K.-I. Jang, S. Y. Heo, K. Cho, H. Luo, B. Zimmerman, J. Kim, L. Yan, X. Feng, S. Xu, M. Fabiani, G. Gratton, Y. Huang, U. Paik, J. A. Rogers, *Sci. Adv.* **2016**, 2, e1600418.
- [12] S. Biswas, Y. Visell, *Adv. Mater. Technol.* **2019**, 4, 1900042.
- [13] M. Lin, N.-G. Gutierrez, S. Xu, *Nat. Electron.* **2019**, 2, 327.
- [14] L.-C. Tai, T. S. Liaw, Y. Lin, H. Y. Y. Nyein, M. Bariya, W. Ji, M. Hettick, C. Zhao, J. Zhao, L. Hou, Z. Yuan, Z. Fan, A. Javey, *Nano Lett.* **2019**, 19, 6346.
- [15] D.-H. Kim, N. Lu, R. Ma, Y.-S. Kim, R.-H. Kim, S. Wang, J. Wu, S. M. Won, H. Tao, A. Islam, K. J. Yu, T.-i. Kim, R. Chowdhury, M. Ying, L. Xu, M. Li, H.-J. Chung, H. Keum, M. McCormick, P. Liu, Y.-W. Zhang, F. G. Omenetto, Y. Huang, T. Coleman, J. A. Rogers, *Science* **2011**, 333, 838.
- [16] S. Wang, J. Y. Oh, J. Xu, H. Tran, Z. Bao, *Acc. Chem. Res.* **2018**, 51, 1033.
- [17] A. Chortos, Z. Bao, *Mater. Today* **2014**, 17, 321.
- [18] N. Münzenrieder, G. Cantarella, C. Vogt, L. Petti, L. Büthe, G. A. Salvatore, Y. Fang, R. Andri, Y. Lam, R. Libanori, D. Widner, A. R. Studart, G. Tröster, *Adv. Electron. Mater.* **2015**, 1, 1400038.
- [19] S. Biswas, A. Schoeberl, Y. Hao, J. Reiprich, T. Stauden, J. Pezoldt, H. O. Jacobs, *Nat. Commun.* **2019**, 10, 4909.
- [20] D. Son, J. Lee, S. Qiao, R. Ghaffari, J. Kim, J. E. Lee, C. Song, S. J. Kim, D. J. Lee, S. W. Jun, S. Yang, M. Park, J. Shin, K. Do, M. Lee, K. Kang, C. S. Hwang, N. Lu, T. Hyeon, D.-H. Kim, *Nat. Nanotechnol.* **2014**, 9, 397.
- [21] Y. Kim, M. Mahmood, Y. Lee, N. K. Kim, S. Kwon, R. Herbert, D. Kim, H. C. Cho, W.-H. Yeo, *Adv. Sci.* **2019**, 6, 1900939.
- [22] Y. Khan, A. E. Ostfeld, C. M. Lochner, A. Pierre, A. C. Arias, *Adv. Mater.* **2016**, 28, 4373.
- [23] S. Xu, Y. Zhang, L. Jia, K. E. Mathewson, K.-I. Jang, J. Kim, H. Fu, X. Huang, P. Chava, R. Wang, S. Bhole, L. Wang, Y. J. Na, Y. Guan, M. Flavin, Z. Han, Y. Huang, J. A. Rogers, *Science* **2014**, 344, 70.
- [24] S. Biswas, A. Schöberl, M. Mozafari, J. Pezoldt, T. Stauden, H. O. Jacobs, *NPG Asia Mater.* **2016**, 8, e336.
- [25] A. K. Bansal, S. Hou, O. Kulyk, E. M. Bowman, I. D. W. Samuel, *Adv. Mater.* **2015**, 27, 7638.
- [26] S. A. Mascaro, H. H. Asada, *IEEE Trans. Rob. Autom.* **2001**, 17, 698.
- [27] Y. Khan, D. Han, A. Pierre, J. Ting, X. Wang, C. M. Lochner, G. Bovo, N. Yaacobi-Gross, C. Newsome, R. Wilson, A. C. Arias, *Proc. Natl. Acad. Sci. USA* **2018**, 115, E11015.
- [28] S. Biswas, J. Reiprich, J. Pezoldt, M. Hein, T. Stauden, H. O. Jacobs, *Flexible Printed Electron.* **2018**, 3, 032001.
- [29] S.-C. Park, S. Biswas, J. Fang, M. Mozafari, T. Stauden, H. O. Jacobs, *Adv. Mater.* **2015**, 27, 3661.
- [30] S. Biswas, M. Mozafari, T. Stauden, H. Jacobs, *Micromachines* **2016**, 7, 54.
- [31] H. Zhang, D. Salo, D. M. Kim, S. Komarov, Y.-C. Tai, M. Y. Berezin, *J. Biomed. Opt.* **2016**, 21, 126006.
- [32] M. Elgendi, *Curr. Cardiol. Rev.* **2012**, 8, 14.
- [33] J. L. Sandell, T. C. Zhu, *J. Biophotonics* **2011**, 4, 773.